Enhanced integrated therapy for breast cancer employing Honokiol-loaded mesoporous polydopamine nanoparticles in conjunction with photothermal effects and low-dose metformin

Cite as: APL Bioeng. **9**, 016115 (2025); doi: 10.1063/5.0256571
Submitted: 6 January 2025 · Accepted: 4 March 2025 ·
Published Online: 19 March 2025

View Online Export Citation CrossMark

Qianqian Du,[1,2,3] Qianfan Zhang,[1,2] Jialing Li,[4] Xiaofei Wang,[1,2,3] Xiangyu Gao,[1,2,3] Guangyuan Tan,[1,2] Qian Feng,[5] Jigang Li,[6,a)] Yanchun Meng,[7,a)] and Yongsheng Yu[1,2,a)]

AFFILIATIONS

[1]Chongqing Institute of Green and Intelligent Technology, Chinese Academy of Sciences, Chongqing, China
[2]Chongqing School, University of Chinese Academy of Sciences, Chongqing, China
[3]Department of Biomaterial, College of Life Sciences, Mudanjiang Medical University, Mudanjiang, China
[4]Department of Ultrasound Diagnosis, Xiangya Hospital, Central South University, Xiangya Road, Changsha, China
[5]Key Laboratory of Biorheological Science and Technology, Ministry of Education, College of Bioengineering, Chongqing University, Chongqing, China
[6]Department of Laboratory, Zibo Central Hospital, Shandong, China
[7]Department of Medical Oncology, Department of Oncology, Phase I Clinical Trial Center, Shanghai Cancer Center, Fudan University, Shanghai, China

[a)]**Authors to whom correspondence should be addressed:** maomao102784@126.com; ycmfdushcc@163.com; and yuyongsheng@cigit.ac.cn

ABSTRACT

Breast cancer remains a significant global health challenge, emphasizing the pressing need for innovative therapeutic approaches. Our thorough research investigates the potential of mesoporous polydopamine nanoparticles (MPDA) as a targeted treatment for breast cancer. Meticulously crafted, these nanoparticles were loaded with honokiol (HK), which is a natural product, and then coated with functionalized hyaluronic acid (HA) to boost their ability to target breast cancer cells that overexpress CD44 receptors. The deep penetrating and photothermal (PTT) composite nanosystem combined with low-dose metformin (Met) improves the efficacy of synergetic therapy against breast tumors. The designed nanosystem exhibited exceptional biocompatibility and stability, suggesting its suitability for therapeutic use. Our *in vitro* studies demonstrated that the nanosystem precisely targeted and penetrated breast cancer cells, resulting in significant cell death. Additionally, *in vivo* studies showed that the nanosystem markedly inhibited tumor growth compared to the control group. This tumor-inhibiting effect was due to the combined action of the encapsulated HK, free Met, and the photothermal effect induced by near-infrared laser irradiation. This combination potently stimulates the expression of cleaved caspase-3 and cleaved PARP proteins, ultimately triggering cell apoptosis and effectively curbing tumor proliferation. Our research not only underscores the promising potential of nanoparticles for targeted breast cancer therapy but also sets the stage for further exploration and development of novel nanomedicine-based therapeutic strategies.

INTRODUCTION

Currently, cancer poses a formidable public health challenge in China and globally,[1] with breast cancer accounting for a staggering 11.7% of all cancer cases.[2] Traditional tumor therapies, such as chemotherapy, surgery, and radiation therapy,[3] are widely practiced but come with significant drawbacks.[4] These include a high risk of tumor recurrence,[5] inadequate targeting, severe systemic toxicity from chemotherapy drugs,[6] and the development of multidrug resistance.[7] Consequently, there is a pressing need for the development of innovative cancer treatment approaches.

Photothermal therapy (PTT) has emerged as a promising approach for tumor treatment, leveraging thermal ablation to effectively eliminate tumor cells.[8] During PTT, photothermal agents absorb external light energy and convert it into substantial heat energy. Given that tumor cells exhibit lower heat resistance compared to normal cells, this heat energy selectively ablates the tumor cells while minimizing adverse effects on surrounding healthy tissues.[9] Among the various light sources, near-infrared (NIR) lasers have gained widespread adoption in PTT due to their exceptional tissue penetrability,[10] high resolution, temporal and spatial adjustability, and precise controllability.[11] Photothermal nanomaterials, characterized by their nanoscale dimensions, large specific surface area, and extended *in vivo* circulation time, offer significant advantages in PTT.[12] These materials can be tailored to target tumor tissues through surface ligand modification and exploit the enhanced permeability and retention (EPR) effect, which facilitates their accumulation within tumor sites.[13] This targeted delivery enhances the efficacy of PTT while further reducing potential side effects on normal tissues.

Dopamine, as a neurotransmitter and vasoactive substance, at low concentrations can cause smooth muscle relaxation by activating D1 receptors, leading to the dilation of renal vessels, mesenteric vessels, and other blood vessels, resulting in blood pressure fluctuations, increased heart rate, or arrhythmia.[14] At high concentrations, dopamine can stimulate α1 receptors, causing contraction of vascular smooth muscle, leading to peripheral vasoconstriction and increased blood pressure.[15] Polydopamine (PDA) is a substance formed by the polymerization of dopamine. Its structure is similar to that of dopamine, but its main function in blood vessels is to form a biocompatible coating. This coating can enhance the biocompatibility, targeting efficiency, and integration with the surrounding tissues of implants, reducing the risk of rejection or inflammation. Furthermore, PDA possesses outstanding photothermal conversion performance,[16] demonstrating strong absorption under 808 nm near-infrared light.[17] This unique property allows it to convert light energy into heat, which can be harnessed for therapeutic purposes such as photothermal therapy.[18] Despite its many advantages, traditional polydopamine nanoparticles have a limitation in their specific surface area, which can restrict their efficacy in drug delivery applications. Compared with PDA, mesoporous polydopamine nanoparticles (MPDA) exhibits a more abundant pore structure and a larger specific surface area, thus possessing the potential for drug delivery.[19] The surface and mesopores of MPDA nanoparticles are rich in a large number of phenyl, amino, and hydroxyl functional groups, which enables them to effectively load various chemical drugs through π–π stacking or hydrogen bonding interactions.[20] In addition, the unique physicochemical properties of MPDA, including its photothermal conversion ability, microenvironment-triggered drug release mechanism, high chemical reactivity, and ease of surface modification, all endow it with application potential in drug delivery systems. The biodegradability and biocompatibility of MPDA ensure its good tolerance *in vivo* and significantly reduce the risk of adverse side effects associated with traditional cancer treatment methods.[21] MPDA can achieve targeted delivery to specific lesion tissues, making it a research focus in the fields of tumor treatment and antibacterial therapy.[22]

Honokiol (HK), a biphenolic compound derived from the outer layer of both *Magnolia officinalis* and their varieties, holds a prominent position as one of the primary medicinal constituents in *Magnolia officinalis*.[23] This remarkable compound possesses a diverse range of pharmacological properties, encompassing antibacterial, antioxidant, anti-inflammatory, antiviral, and antitumor activities. It exerts profound effects on various physiological systems, including the digestive, nervous, cardiovascular, and respiratory systems.[24] Recently, honokiol has garnered significant attention due to its potential to induce apoptosis and manage malignant tumors, making it a highly promising candidate for anticancer drug development.[25] Its ability to target multiple pathways and mechanisms within cancer cells underscores its potential as a multifaceted therapeutic agent. Notably, HK demonstrates exceptional bioavailability, easily crossing the blood–brain and blood–spinal fluid barriers, making it an attractive option for treating brain and spinal cord tumors.[26] The antitumor efficacy of HK is characterized by its multi-target and multi-linkage approach, with low toxicity and potent anti-proliferative effects on a wide range of cancer cells.[27] However, despite its promising therapeutic potential, the challenges posed by HK's limited water solubility and low oral bioavailability have hindered its development and clinical application. These issues have restricted the compound's ability to reach effective concentrations at tumor sites, thereby limiting its efficacy. Consequently, there is an urgent need for an effective method to deliver HK to tumor sites, overcoming the barriers posed by its physicochemical properties.[28] Researchers are actively exploring various delivery strategies, such as encapsulation in nanoparticles or liposomes, to enhance the solubility, stability, and bioavailability of HK, thereby unlocking its full therapeutic potential.[29] The development of such delivery systems could pave the way for the successful translation of HK from the laboratory to the clinic, ultimately benefiting patients with a wide range of cancers.

In the realm of tumor biology, metformin (Met) has demonstrated the capacity to target multiple signaling cascades implicated in cancer development and progression.[30] However, the mechanisms by which Met exerts its antitumor effects are multifaceted and not fully understood. One key aspect of Met's antitumor activity involves the induction of apoptosis, a series of molecular events that lead to the activation of caspase enzymes, which are critical for the proteolytic cleavage of cellular substrates, ultimately resulting in cell death.[31] Research has shown that Met can induce the cleavage of caspase-3 and PARP in various cancer cell lines, including breast, prostate, and pancreatic cancers.[32] These findings support the notion that Met may exert its antitumor effects, in part, through the activation of the apoptotic pathway.

In pursuit of enhancing the drug loading efficiency of PDA-based nanoparticles, we meticulously designed and synthesized MPDA nanoparticles using an efficient one-pot method, as illustrated in Scheme 1. These engineered nanoparticles were employed as carriers for HK, which was effectively encapsulated within their structure through a combination of electrostatic interactions and π–π stacking. This encapsulation strategy not only maximized the loading capacity but also ensured the stable retention of HK within the MPDA nanoparticles. To augment the responsiveness and targeting precision of MPDA toward the tumor microenvironment, we adopted a dual modification approach. PDA was combined with hyaluronic acid (HA), leveraging their unique properties to enhance interactions with tumor cells. This modification not only enhanced the biocompatibility and stability of the drug-loaded MPDA but also promoted its recognition and binding to specific receptors on cancer cell surfaces, thereby improving its targeting capabilities. To evaluate the antitumor activity

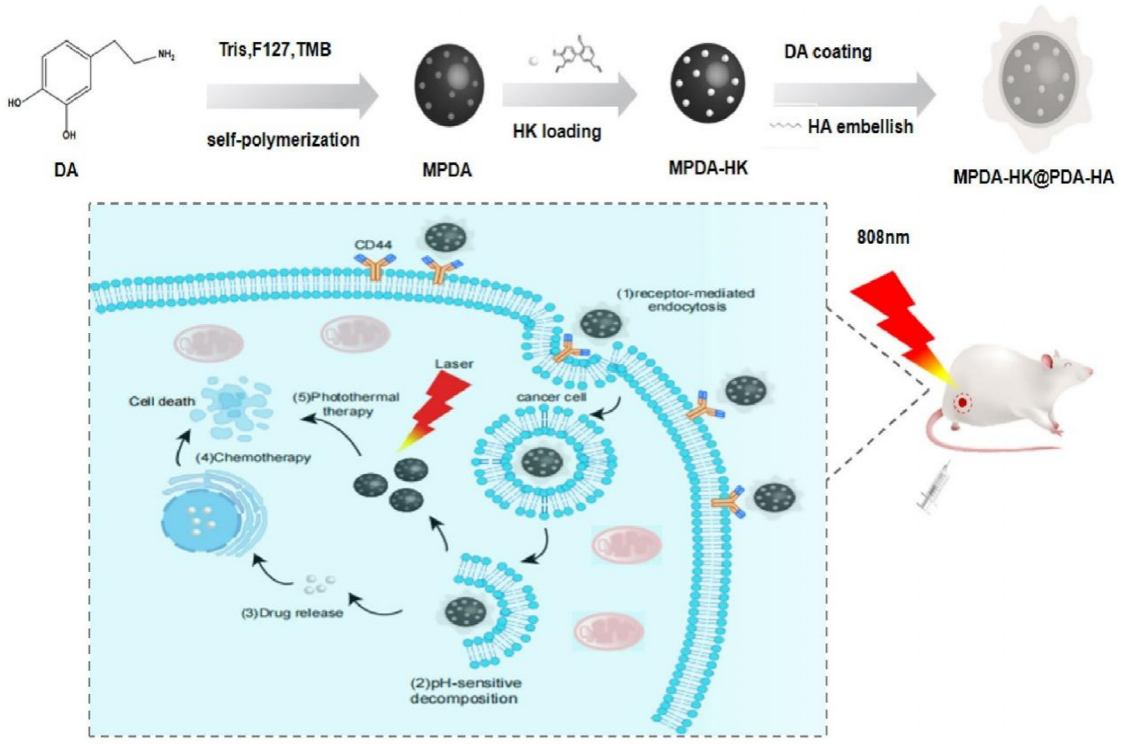

SCHEME 1. Schematic illustration of MPDA-HK@PDA-HA nanoparticles targeting pH response for drug/photothermal synergistic tumor therapy.

of the modified MPDA *in vitro*, we conducted experiments using human breast cancer cells (MCF-7) and mouse breast cancer cells (4T1). The results were promising, indicating that the modified MPDA could effectively inhibit cancer cell proliferation. Furthermore, we assessed the efficacy of metformin in combination with MPDA-HK@PDA-HA as a potential *in vivo* antitumor therapy. This combination therapy aimed to harness the synergistic effects of Met and the modified MPDA, with the goal of achieving more potent antitumor activity and better patient outcomes. Collectively, these findings lay the groundwork for further research and development of advanced antitumor therapies utilizing MPDA nanoparticles.

RESULTS AND DISCUSSION

Preparation and characterization of MPDA-HK@PDA-HA

In this investigation, MPDA NPs were successfully synthesized through the polymerization of dopamine at the interface of an emulsion template, employing a method previously documented in the literature.[33] By utilizing Pluronic F127 and TMB as organic templating agents, dopamine underwent self-polymerization to form PDA within an alkaline milieu, facilitated by the catalysis of ethanol and Tris. This process was driven by π–π stacking interactions stemming from the TMB. The removal of the templating agents subsequently led to the formation of a mesoporous structure. Honokiol (HK), a hydrophobic compound, was efficiently loaded into MPDA *via* π–π stacking and hydrogen bonding interactions, resulting in the formation of MPDA-HK. Subsequently, the functionalization of MPDA-HK was achieved through the self-polymerization of dopamine and hyaluronic acid (HA) under mild alkaline conditions, which enriched the functional interactions between them. The MPDA-HK@PDA-HA nanomedical drugs that were designed and synthesized in this study aim to enhance the targeting efficacy toward tumors, prevent premature drug release, and synergize with photothermal therapy for comprehensive tumor treatment.

As depicted in [Fig. 1(a)], the SEM images of MPDA NPs reveal an average diameter of approximately 100 nm, exhibiting a consistent and uniform spherical morphology. Upon loading HK and modifying with HA [Figs. 1(b) and 1(c)], the nanoparticles maintain their size and shape with minimal alteration. Furthermore, TEM analysis confirms the presence of uniformly distributed mesoporous surfaces on the MPDA NPs [Fig. 1(d)]. However, these mesoporous features diminish upon drug loading and modification, as illustrated in [Figs. 1(e) and 1(f)]. The particle size measurements depicted in [Fig. 1(g)] indicate that the hydrated diameter of MPDA NPs is 313 nm, with a slight increase to 350 nm following drug loading and modification. The surface zeta potential of the NPs undergoes a shift from −21.77 mV for MPDA NPs to −27.47 mV for MPDA-HK@PDA-HA, potentially attributed to the incorporation of negatively charged hyaluronic acid during surface modification [Fig. 1(h)]. Fourier transform infrared (FTIR) spectroscopy results exhibit characteristic peaks of HK and HA within the ranges of 3010–3030 and 1650–1690 cm^{-1}, respectively, providing additional evidence for the successful loading of HK and modification with HA [Fig. 1(i)].

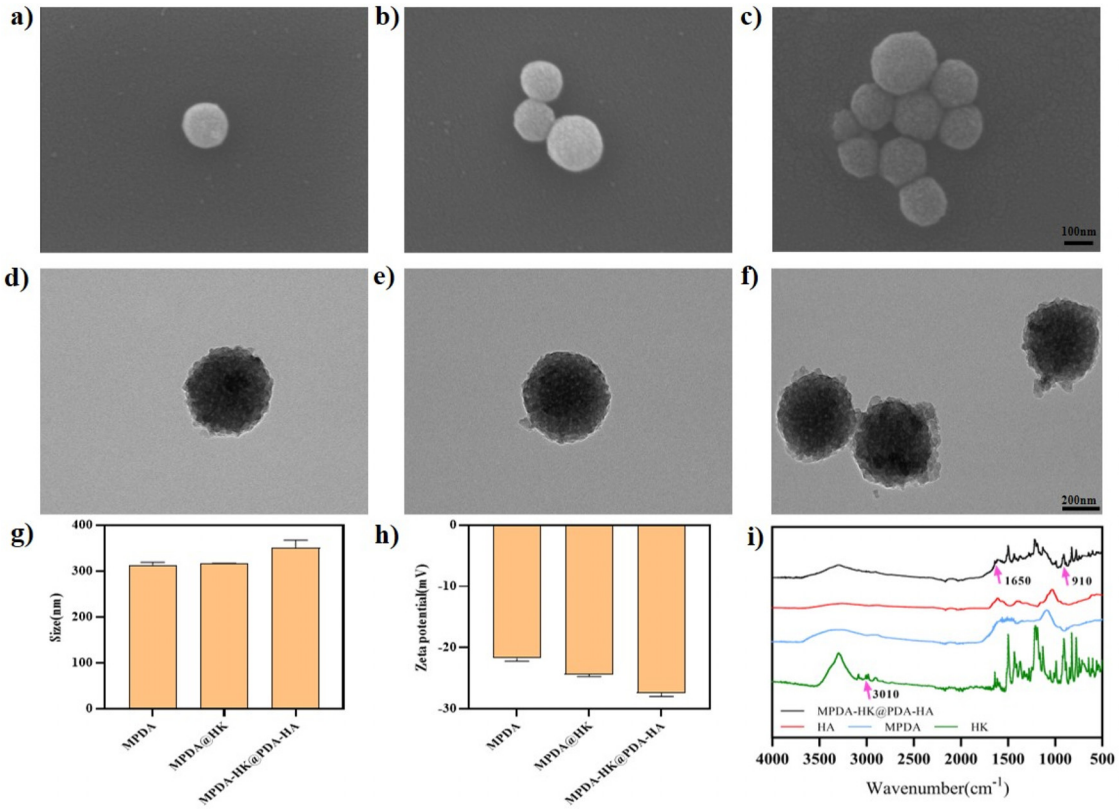

FIG. 1. SEM photos of (a) MPDA NPs, (b) MPDA@HK NPs, and (c) MPDA-HK@PDA-HA NPs. Scale bar: 100 nm. TEM photos of (d) MPDA NPs, (e) MPDA@ HK NPs, and (f) MPDA-HK@PDA-HA NPs. Scale bar: 200 nm. (g) The particle size (h) and surface Zeta potential of MPDA NPs, MPDA@HK NPs, and MPDA-HK@PDA-HA NPs. (i) FTIR images of HK, HA, MPDA, and MPDA-HK@PDA-HA.

Drug release and photothermal properties of MPDA

MPDA NPs have attracted significant attention as highly potent drug carriers, owing to their distinctive pore size and considerable specific surface area. [Fig. 2(a)] displays the N_2 adsorption–desorption curve of MPDA NPs, which, according to IUPAC classification, exhibits a type IV isotherm. The BET test data presented in [Fig. 2(b)] reveals that the MPDA NPs possess a specific surface area of approximately 32.81 m^2/g and a total pore volume of 0.082 cm^3/g, indicating their exceptional drug loading capacity. By utilizing high-performance liquid chromatography to detect the HK concentration, we were able to determine the drug concentration through peak area measurement. The encapsulation rate and drug loading results depicted in [Fig. 2(c)] demonstrate that MPDA NPs achieve a remarkable HK encapsulation rate of 74.54% and a drug loading of 26.44%, further affirming their high load efficiency. One of the limitations of HK is its poor water solubility; however, MPDA-loaded HK can be precisely targeted to deliver the drug to the tumor site and efficiently release it. [Figure 2(d)] shows the HK release profile of MPDA-HK@PDA-HA. Due to the protective coating of HA, HK avoids premature leakage and rapid release. Additionally, the acidic microenvironment influences its release, causing HK to be more fully released in such conditions. Specifically, at a pH of 7.4, 58% of the drug is released, whereas at a pH of 5.5, 82% of HK is released.

MPDA NPs excel as photothermal agents in PTT, thus rendering the assessment of their photothermal conversion performance and efficiency a pivotal benchmark. To delve into the photothermal attributes of MPDA, we measured the temperature variations in MPDA solutions of varying concentrations upon exposure to 1 W/cm^2 of 808 nm near-infrared radiation for 10 min. [Figure 2(e)] illustrates that as the MPDA concentration escalates, the temperature climbs more rapidly upon illumination, achieving an impressive temperature rise of 56.7 °C, thereby demonstrating a concentration-dependent behavior. [Figure 2(f)] depicts the temperature alterations in a 1 mg/ml MPDA solution when subjected to NIR radiation of different power intensities. Notably, the magnitude of temperature change intensifies with increasing illumination power, showcasing a clear power density dependence. To ascertain the impact of MPDA modification on its photothermal conversion capabilities, we compared the temperature changes between unmodified MPDA and MPDA-HK@PDA-HA at an equivalent concentration. As evident from [Fig. 2(g)], the modified MPDA retains its robust photothermal conversion capability, albeit without significant alteration. Finally, to evaluate the stability of MPDA's photothermal effect, we subjected a 500 μg/ml MPDA solution to repeated laser irradiation at 1 W/cm^2 for three cycles, each spanning 10 min. [Figure 2(h)] presents the results, revealing that the liquid temperature consistently attains its peak during the initial irradiation cycle. This

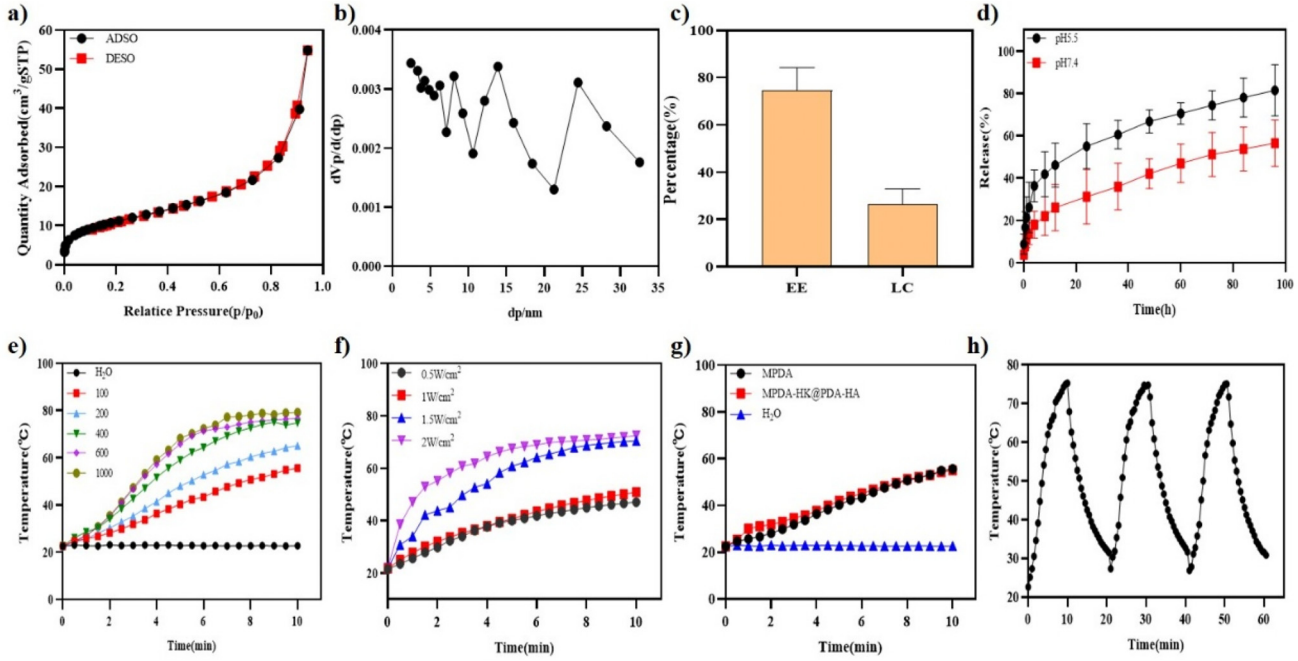

FIG. 2. Nitrogen adsorption isotherm of MPDA NPs. (a) Corresponding pore size distribution. (b) and (c) Drug loading and encapsulation rate of MPDA. (d) Drug response release curve of MPDA-HK@PDA-HA. (e) Temperature change curve of H_2O, MPDA (100, 200, 400, 600, and 1000 μg/ml) under 808 nm laser irradiation (1 W/cm^2). (f) Temperature rise curve of 1000 μg/ml MPDA in H_2O under NIR laser with different powers (0.5, 1.0, 1.5, and 2.0 W/cm^2). (g) Temperature rise curve of MPDA, MPDA-HK@PDA-HA, and H_2O solutions under near-infrared radiation of 1 W/cm^2. (h) Thermal stability curve of 500 μg/ml MPDA suspended in H_2O under three cycles of on/off near-infrared (1 W/cm^2) laser treatment.

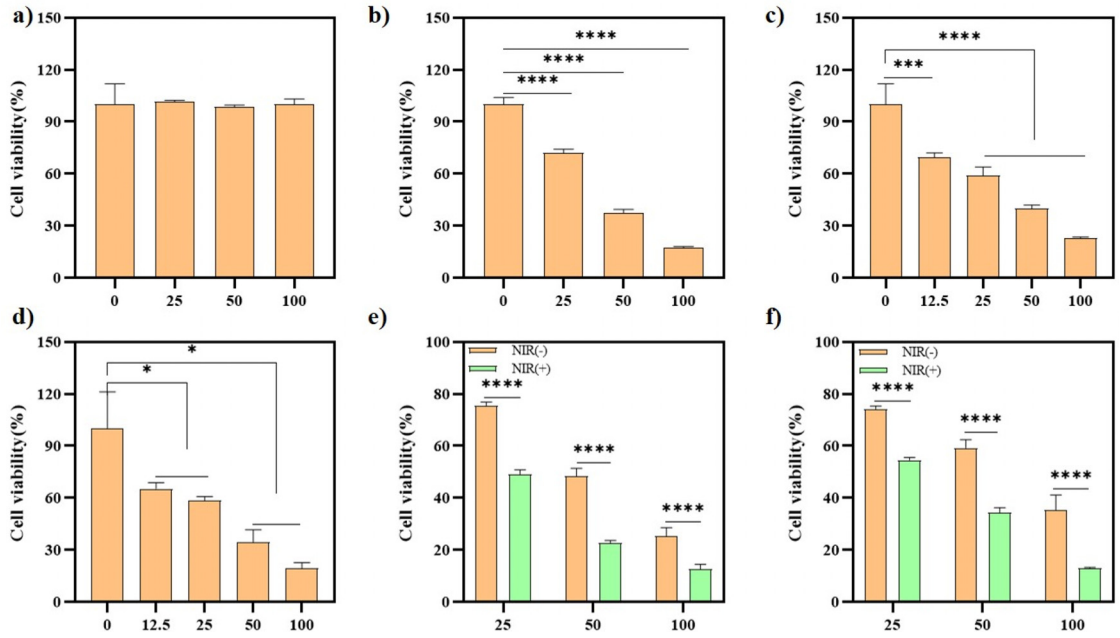

FIG. 3. The survival rate of MCF-7 cells treated with MPDA (a) and HK (b) at different concentrations. The survival rates of 4T1 cells (c) and MCF-7 cells (d) after treatment with different concentrations of MPDA-HK@PDA-HA. Survival rates of 4T1 cells (e) and MCF-7 cells (f) with or without NIR irradiation (808 nm, 1 W/cm^2, 5 min). $^*p < 0.05$, $^{***}p < 0.001$, and $^{****}p < 0.0001$.

underscores the photothermal effect's substantial stability and commendable reproducibility.

Biocompatibility of MPDA-HK@PDA-HA

In biomedical applications, the cellular and blood compatibility of nanodrug delivery systems is critical. As illustrated in [Fig. 3(a)], the MPDA solution exhibited minimal toxicity toward MCF-7 cells at the tested concentrations. By examining the cytotoxicity of HK against MCF-7 cells, [Fig. 3(b)] reveals that HK possesses a significant cell-killing effect on these cells. Cytotoxicity experiments were further conducted on both MCF-7 and 4T1 cells to assess the toxicity of MPDA-HK@PDA-HA. The results, presented in [Figs. 3(c) and 3(d)], indicate that MPDA-HK@PDA-HA demonstrated a robust tumor cell-killing effect on both cell lines at the tested concentrations. Specifically, at a liquid concentration of 100 μg/ml, the survival rate of both breast cancer cell types dwindled to approximately 20%.

To demonstrate a synergistic effect between HK and photothermal therapy, we examined the cytotoxicity of MPDA-HK@PDA-HA with or without near-infrared laser irradiation. As shown in [Figs. 3(e) and 3(f)], when the concentration of MPDA-HK@PDA-HA is 100 μg/ml, the survival rate of 4T1 cells without near-infrared irradiation is 25.25%, and after photothermal treatment, the cell viability is reduced to 12.56%, while the survival rate of MCF-7 cells is reduced from 35.19% to 12.98%. The effect of HK increased with the increase in concentration. These results indicate that MPDA-HK@PDA-HA can achieve the synergistic therapeutic effect of chemotherapy and photothermal PTT by absorbing near-infrared laser to produce a thermal effect.

Nanomaterials, as carriers for drug release, inevitably come into contact with erythrocytes during biological transportation. Therefore, good blood compatibility is a must-have property for nano. In this study, fresh rabbit blood erythrocytes were used to test the hemolytic toxicity of different concentrations of MPDA-HK@PDA-HA. As shown in [Fig. S1(a)], it can be visualized that the supernatants of the negative control and experimental groups were clear and there was no release of hemoglobin. While almost all red blood cells in the positive control group were ruptured. The specific hemolysis rate is shown in [Fig. S1(b)], and the hemolysis rate of the MPDA-HK@PDA-HA group is below 5%, which indicates that they are less destructive to erythrocytes and have good blood compatibility.

To further clarify the application potential of MPDA-HK@PDA-HA, its pharmacological properties were preliminarily evaluated. By intravenously injecting MPDA-HK@PDA-HA into mice, the changes in its blood drug concentration over time were detected. As shown in [Fig. S2], the concentration of MPDA-HK@PDA-HA in the blood rapidly decreased over time. After fitting and calculation, its half-life ($t_{1/2}$) was only 4.74 min. The drug circulates through the blood to reach the heart, liver, spleen, lungs, and kidneys. The drug concentration was the highest in the heart, and then it was rapidly excreted through the kidneys.

Cell uptake of MPDA-HK@PDA-HA in tumor cells

The endogenous capacity of MPDA-HK@PDA-HA cells was investigated using MCF-7 cells. The uptake capacity of free C-6, MPDA-C-6, and MPDA-C-6@PDA-HA cells was observed using C-6 and C-6-labeled MPDA and MPDA-HK@PDA-HA, respectively. After incubation with drugs, the cells could be observed under confocal laser microscopy, as shown in [Figs. 4(a) and 4(b)]. Apparent and robust green fluorescence was observed in the cytoplasm of the MPDA-C-6@PDA-HA group, while weak green fluorescence was observed in the cells of the C-6 and MPDA-C-6 groups. These results indicate that HK can effectively enter the cells through the encapsulation of MPDA-HK@PDA-HA, laying the foundation for the subsequent drug release to exert tumor therapeutic effects. Since the CD44 receptor is highly expressed in 4T1[34] and MCF-7[35] breast cancer cells but lowly expressed in normal cells such as L929[36] cells, after external

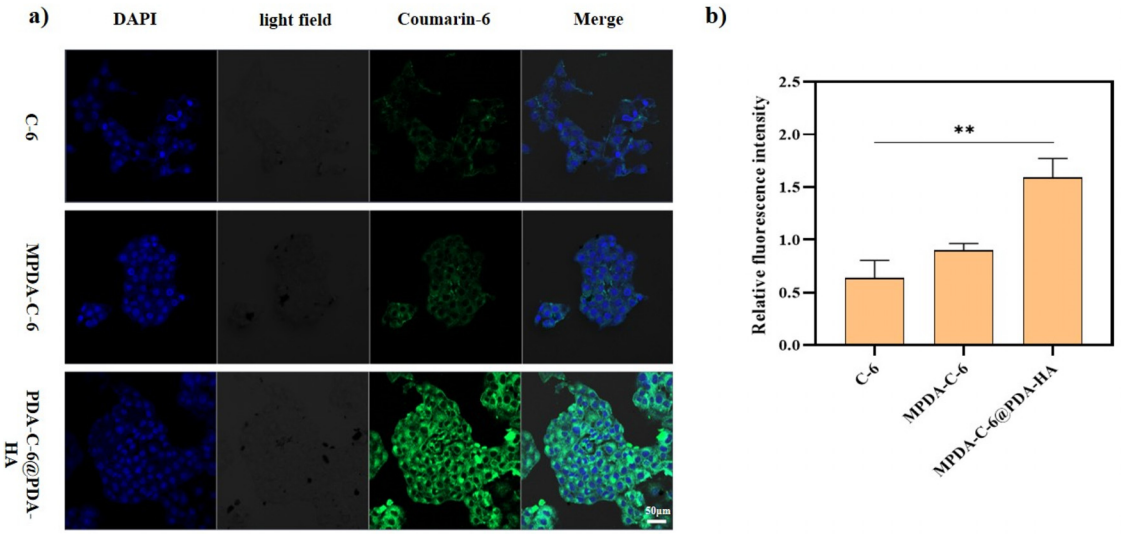

FIG. 4. (a) Cellular uptake of free C-6, MPDA-C-6, MPDA-C-6@PDA-HA, MPDA labeled with C-6. Nuclear staining with DAPI. (b) The relative fluorescence intensity of C-6, MPDA-C-6, and MPDA-C-6@PDA-HA. Scale bar: 50 μm, $^{**}p < 0.01$.

modification with HA, HA can target the highly expressed CD44 receptor on the tumor cell membrane, making the constructed MPDA-HK@PDA-HA have a stronger targeting effect, which is conducive to the uptake of tumor cells.

In vivo antitumor activity of MPDA-HK@PDA-HA

Since cytotoxicity experiments *in vitro* demonstrated the promising antitumor efficacy of MPDA-HK@PDA-HA, it becomes imperative to delve deeper into its antitumor activity *in vivo*. Tumor-bearing mice were randomly divided into five different groups: the PBS group, the HK group, the MPDA+NIR group, the MPDA-HK@PDA-HA group, and the MPDA-HK@PDA-HA+NIR group. When the tumor volume reached 100 mm^3, various drugs were administered *via* tail vein injection. For the groups receiving light irradiation, an 808-nm laser (with a power of 1 W/cm^2 for 5 min) was applied the next day [Fig. S3(a)]. There was a significant difference in tumor volume between the treatment groups and the control group, and the treatment groups showed the best tumor suppression effect [Fig. S3(b) and S3(c)]. As shown in [Fig. S3(d)], the mice were euthanized after eight days of treatment, and the tumor tissues were collected and photographed. The temperature change curve of the near-infrared group shown in [Fig. S3(e)] confirmed that the MPDA nanoparticles had excellent photothermal conversion ability in mice, efficiently converting near-infrared light absorption into heat energy, generating high temperatures, and ultimately eliminating tumor cells. Additionally, the body weight of mice in all groups remained stable during the drug administration period, indicating that the drugs in each group caused minimal toxicity [Fig. S3(f)].

The *in vivo* multi-faceted activity of MPDA-HK@PDA-HA in combination with metformin (Met)

The breast cancer tumor-bearing mice were randomly divided into five groups: PBS, MPDA-HK@PDA-HA, MPDA-HK@PDA-HA + NIR, MPDA-HK@PDA-HA + Met, and MPDA-HK@PDA-HA + Met + NIR. To further enhance the *in vivo* antitumor efficacy of MPDA-HK@PDA-HA, it was co-administered with low-dose metformin (20 mg/kg) for therapeutic intervention.[37] As illustrated in [Fig. 5(a)], the mice were intravenously injected *via* the tail vein with 100 μl of the corresponding drug on day 1, followed by irradiation with an 808 nm near-infrared laser at a power density of 1 W/cm^2 for 5 min on day 2. This treatment regimen was repeated over a total period of 8 days. [Figure 5(b)] indicates that the MPDA-HK@PDA-HA+Met+NIR group demonstrated the most potent inhibitory effect on breast cancer growth, significantly surpassing the other groups. After 8 days, the mice were euthanized, and their tumor tissues were collected and weighed. [Figures 5(c) and 5(d)] further indicate that the tumor weight in the MPDA-HK@PDA-HA+Met+NIR group was the lightest, further confirming that the combined use of MPDA-HK@PDA-HA, metformin, and near-infrared therapy had the best antitumor effect. Additionally, throughout the drug administration period, the body weight of all groups of mice remained stable, indicating that the toxicity of the drugs in each group was extremely low [Fig. 5(e)].

To further investigate the antitumor effects of MPDA-HK@PDA-HA and Met *in vivo*, we performed apoptosis analysis of tumor histologic sections by hematoxylin and eosin (H&E) and TDT-mediated dUTP nickel end labeling (TUNEL) staining. As shown in [Fig. 6], HE staining showed that the cell density in the tumor tissues treated with PBS and HK was significant, with round

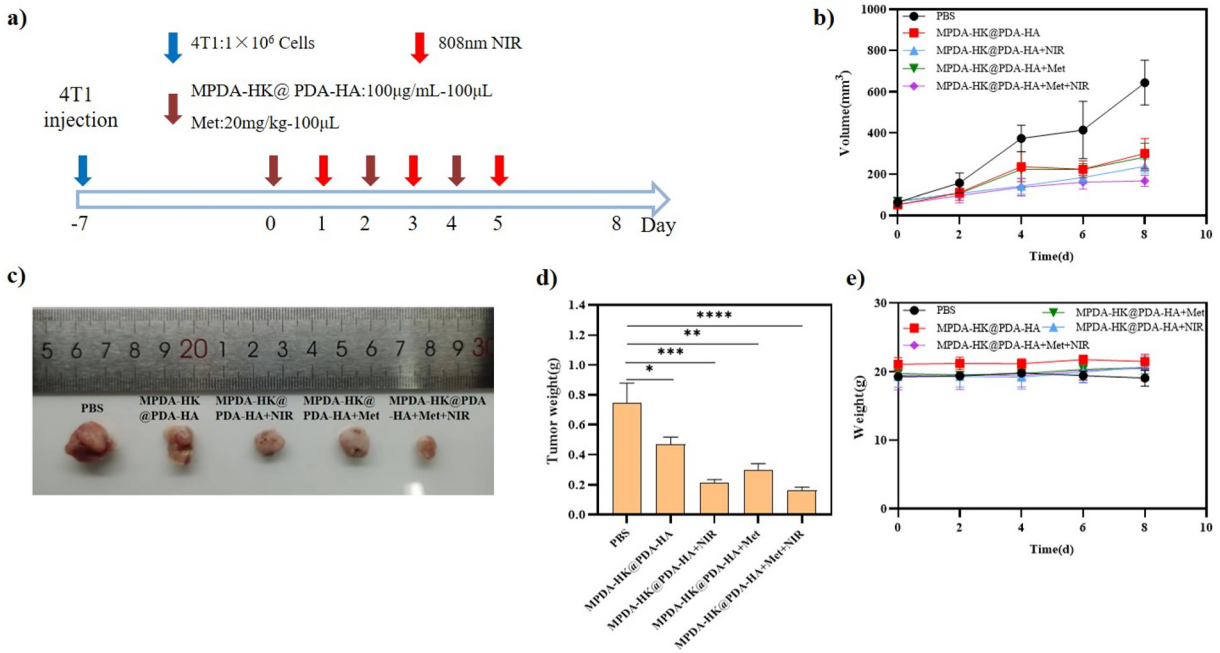

FIG. 5. (a) An illustration depicts the therapeutic procedure. (b) Changes in tumor volume during treatment. (c) Representative pictures of tumor volume in each group after treatment. (d) Tumor weight at the end of treatment. (e) Changes in body weight during treatment. $^{*}p < 0.05$, $^{**}p < 0.01$, $^{***}p < 0.001$, and $^{****}p < 0.0001$.

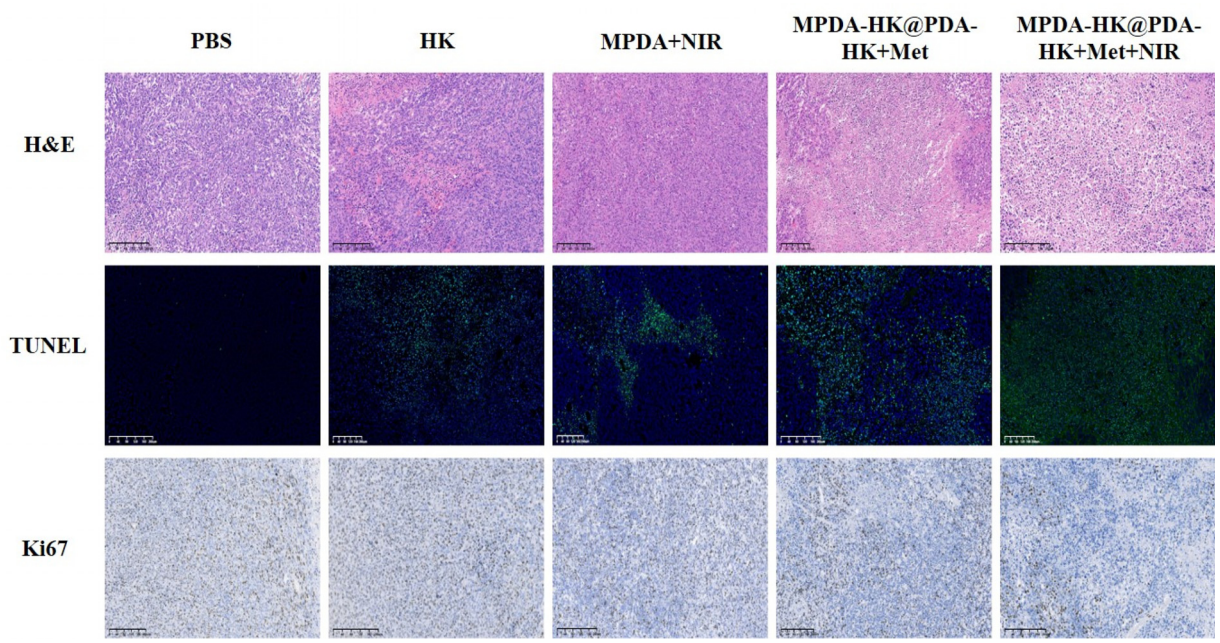

FIG. 6. H&E, TUNEL, and Ki67 staining images of different treatment groups. Scale bar: 100 μm.

and dense nuclei, and sporadic apoptosis and necrosis were observed, indicating that the killing effect of HK on tumor cells was weak. The tumor cell density in the MPDA+NIR group was relatively high, and some cells showed apoptosis and necrosis. The MPDA-HK@PDA-HA+Met +NIR treatment group caused significant tumor tissue cell necrosis, characterized mainly by nuclear pyknosis, nuclear rupture, and nuclear adhesion. Compared with the HK treatment group, MPDA-HK@PDA-HA+Met+NIR showed more extensive apoptosis and necrosis. In addition, HE staining images revealed scattered necrotic areas of chromatin and nucleoli, as well as extensive lymphocyte infiltration into the tumor tissue and connective tissue. The results of the TUNEL assay also indicated that the apoptosis of tumor cells in the MPDA-HK@PDA-HA+Met+NIR group was significantly higher than that in other treatment groups. In addition, the tumor sections of each group were stained with Ki67 immunofluorescence. The MPDA-HK@PDA-HA+Met+NIR group had the smallest green fluorescent region, indicating that the growth of mouse tumor cells in the MPDA-HK@PDA-HA+Met+NIR group was the most inhibited, and therefore the expression of nuclear protein related to cell proliferation was the lowest. In summary, MPDA-HK@PDA-HA combined with metformin and PTT synergistic chemotherapy have good inhibition and therapeutic effects on tumor growth *in vivo*. After treatment, HE staining was performed on the heart, liver, spleen, lung, and kidney of mice in each group, as shown in [Fig. S4]. No obvious abnormalities were found in the histological structure and cell morphology of mice in each group. It shows that our nanoparticles have good biocompatibility and will not cause toxic side effects.

Mechanism of apoptosis in Met cells

Metformin is a traditional hypoglycemic drug. However, studies have found that using metformin in a fasting state can significantly inhibit tumor growth. Through Western blot (WB) experiments, we verified that Met inhibited the caspase 3/PARP signaling pathway of MCF-7 cell apoptosis. As shown in [Fig. 7(a)], MCF-7 cells treated with metformin at 1, 5, 10, and 20 mM concentrations for 48 h decreased the expression of caspase 3 and PARP proteins with the increase in metformin concentration compared with the control group without treatment. The protein expression levels of cleaved caspase 3 and cleaved PARP increased with the increase in metformin concentration. After 1 mM metformin treatment, MCF-7 cells could only detect weak cleaved PARP protein, indicating that the apoptosis of MCF-7 cells was very low at 1 mM metformin concentration. The WB results of relative animal tissues are shown in [Fig. 7(b)]. The expression levels of caspase 3 and PARP in the metformin-treated group were the lowest, and the proteins of caspase 3 and PARP were increased, respectively. Therefore, metformin inhibits the expression of caspase 3 and PARP proteins, stimulates the expression of cleaved caspase 3 and cleaved PARP proteins, induces cell apoptosis, and thus inhibits tumor growth.

CONCLUSION

In order to effectively treat breast cancer, a multifunctional nanomaterial was prepared for microenvironment response and tumor-targeted breast cancer photothermal therapy. *In vitro* experiments, HK-loaded MPDA nanoparticles can effectively kill breast cancer cells, and the antitumor effect is further improved under 808 nm near-infrared irradiation. Cell uptake experiments showed that the MPDA nanoparticles modified with hyaluronic acid had apparent tumor targeting and could effectively accumulate in the tumor. *In vivo* experimental studies, PTT therapy with drug-loaded MPDA nanoparticles combined with low-dose metformin appears more effective in inhibiting tumor growth than individual therapy. This indicates that compared with single chemotherapy or photothermal therapy,

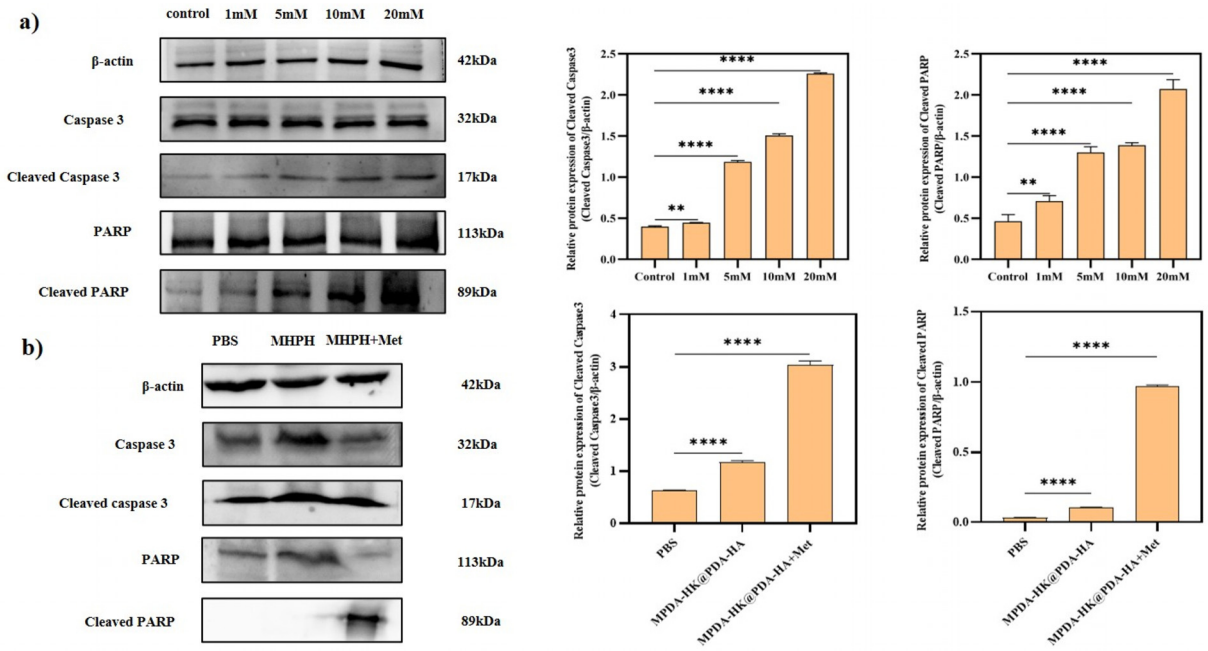

FIG. 7. (a) Expression of related proteins after treatment with metformin at different concentrations (left panel); quantification of cleaved caspase3 and cleaved PARP (right panel). (b) Expression of related proteins in mice after different treatments (left panel); quantification of cleaved caspase3 and cleaved PARP (right panel). $^{**}p < 0.01$ and $^{****}p < 0.0001$.

photothermal therapy combined with chemotherapy shows a significant synergistic therapeutic effect, and the antitumor mechanism of metformin has been further verified. The integration of these agents may pave the way for personalized and advanced treatment strategies that address the complex challenges associated with breast cancer.

METHODS

Materials

Honokiol (HK) was purchased from Aladdin Biochemical Technology Co., LTD (Shanghai, China). Dopamine hydrochloride, 1,3,5-trimethylbenzene (TMB), Pluronic F127, and Tris (hydroxymethyl) aminomethane (Tris) were purchased from McLean Biochemical Technology Co., LTD (Shanghai, China). DMEM culture medium was purchased from Thermofisher (Shanghai China). The remaining reagents are analytically grade reagents and do not require further purification.

Cells and animals

Human breast cancer cells (MCF-7) and mouse breast cancer cells (4T1) were obtained from Cell Bank/Stem Cell Bank, Chinese Academy of Sciences. Female Balb/c mice were purchased from Chongqing Ensville Biotechnology Co., LTD (Chongqing, China).

Synthesis of MPDA nanoparticles

According to the literature review, mesoporous polydopamine nanoparticles (MPDA NPs) were synthesized by the one-pot method. 60 ml H_2O and 60 ml ethanol were mixed into a 250 ml round flask, 370 mg F127 and 400 μl TMB were added to the above solution, and then the solution was stirred for 30 min to be dissolved. Then, 100 mg TRIS solution (5 ml water) and 100 mg dopamine hydrochloride solution (1 ml DI water) were added successively. The reaction was performed at room temperature for 24 h, and then 100 ml acetone was added and stirred. The mixture was centrifuged at 11 000 rpm for 15 min at 4 °C and then re-suspended with acetone/ethanol (1:2, v/v) and ultrasonic precipitation for 30 min. The supernatant was centrifuged and repeated three times. The synthesized MPDA NPs were collected by high-speed centrifugation, and the collected precipitate was dried in an oven at 37 °C.

Preparation of MPDA-HK@PDA-HA NPs

MPDA NPs and HK were dispersed in ultra-pure water at a mass ratio of 1:5 and stirred for 24 h to load the drug. HK gradually accumulated in mesoporous polydopamine through π–π accumulation and hydrophilic/hydrophobic action. The 1 mg MPDA-HK nanoparticles were dispersed in Tris (10 mmoL, pH 8.5) buffer solution, added with an appropriate amount of PDA and HA, stirred at 37 °C for 4h, centrifuged at 13 000 rpm for 10 min, and the precipitation was collected. In the same way, HK was changed into coumarin 6 (C-6), and fluorescent nanoparticles MPDA-HK@PDA-HA-C-6 were synthesized.

Scanning electron microscopy of nanoparticles

Appropriate amounts of nanoparticles were taken, sprayed with gold for 80 s, and then the floating powder was blown away and imaged under a scanning electron microscope at 5 kV.

Transmission electron microscope

The appropriately diluted nanoparticles were absorbed and dropped on the copper mesh, respectively. After settling for 30 min, the excess float was absorbed with filter paper, left to dry, and imaged under a transmission electron microscope at 200 kV.

Fourier transform infrared spectral analysis

The characteristic functional groups of HA, HK, MPDA, and MPDA-HK@PDA-HA were analyzed by infrared spectroscopy. All samples for infrared analysis were freeze-dried into powder samples using the Cary 630 infrared spectrometer. The ATR method recorded spectral data from 4000 to 400 cm^{-1}, and the measured signal resolution was 2 cm^{-1} absorption.

Loading rate and encapsulation rate

Magnolol was analyzed by high-performance liquid chromatography (HPLC) under the following conditions: C18 column was used with a mobile phase consisting of acetonitrile/water (70:30, v/v), the flow rate was 1 ml/min, the sample size was 50 μl, the detection wavelength was 254 nm, and the column temperature was 30 °C. The supernatant after MPDA-HK was collected by centrifugation and filtered and the HK content was detected by HPLC. The dosage of the drug in the preparation is Wh, and the total weight of the drug-loaded nanoparticles is Wt. The formula for the loading rate is as follows:

$$\text{Drug load}(\%) = \frac{\text{Wh}}{\text{Wi}} \times 100. \quad (1)$$

The amount of free drug is denoted as A0, while the total amount of added drug is represented by At. The formula for calculating the encapsulation efficiency is presented as follows:

$$\text{Encapsulation rate}\,\% = 1 - \frac{\text{A0}}{\text{At}} \times 100. \quad (2)$$

Drug release studies *in vitro*

1 mg MPDA-HK@PDA-HA was added into a centrifuge tube and then suspended in 2 ml PBS buffer solution containing 0.5% Tween-80. The centrifuge tube was then placed in a water bath at 37 °C for a drug release study *in vitro*. At a predetermined time point (0, 0.5, 1, 2, 4, 8, 12, 24, 36, 48, 60, 72, 84, and 96 h), an equal amount (1 ml) of PBS buffer was removed and an equal volume of fresh PBS solution was added. The sample was centrifuged at 13 000 rpm for 10 min to exclude nanoparticles. The supernatant was filtered by a 0.22 μm filter head and the HK release was determined by HPLC. Each experiment was repeated three times.

Study on cytotoxicity of MPDA-HK@PDA-HA

Cell Counting Kit-8 (CCK-8) was used to detect the cytotoxicity of HK, MPDA, and MPDA-HK@PDA-HA on 4T1 cells and MCF-7 cells. MCF-7 and 4T1 cells were inoculated into 96-well plates with a density of 1×10^4 cells/well, and incubated for 24 h. HK, MPDA, and MPDA-HK@PDA-HA were dissolved or dispersed in dimethyl sulfoxide (DMSO), respectively, and then diluted into a series of concentrations by the medium. A medium of mixed drugs was added to the Petri dish to keep the final concentration of DMSO below 0.1%. The cells were incubated for 24 h and incubated with 10% CCK-8 reagent for 2 h. The absorbance was measured at 450 nm, and the cell survival rate was calculated based on this. Each experiment was repeated three times.

Apoptosis analysis after laser irradiation

4T1 and MCF-7 cells (1×10^4 cells/well) were inoculated on 96-well plates and incubated for 24 h. Fresh medium containing different concentrations of MPDA-HK@PDA-HA was added, incubated for 12h, and irradiated with an 808 nm near-infrared laser (1 W/cm^2) for 5 min or no irradiation. After continuing incubation for 12 h, each well was incubated with 10% CCK-8 reagent for 2 h, and absorbance was detected at 450 nm to evaluate the cell viability.

Cell uptake study

To determine the cellular uptake behavior of MPDA-HK@PDA-HA in tumor cells, the fluorescent dye coumarin 6 (C-6) was embedded in the mesopore of MPDA. MCF-7 cells were inoculated (5×10^5 cells/well) in confocal Petri dishes and incubated for 12 h. The cells were then placed in a fresh medium containing free C-6, MPDA-C-6, and MPDA-C-6@PDA-HA, incubated for 2 h, washed three times with PBS, fixed with 4% paraformaldehyde, and stained with DAPI. After mass washing with PBS, the cells were observed under confocal laser microscopy.

Blood compatibility

Take fresh rabbit blood, centrifuge at 2000 rpm for 3 min, discard the supernatant, wash twice with physiological saline, and collect the precipitate. Then resuspend the rabbit red blood cells with physiological saline to prepare the blood cell suspension. Dilute MPDA-HK@PDA-HA with physiological saline to a final concentration of 12.5–100 μg/ml. Add the same volume of the blood cell suspension and different concentrations of MPDA-HK@PDA-HA to sterile tubes, with PBS as the negative control and 0.1% Triton-X100 as the positive control. Cultivate in a 37 °C constant temperature incubator for 1 h, then centrifuge at 2000 rpm for 5 min, take pictures, and record. Take the supernatant and put it into a 96-well plate, measure the absorbance at 450 nm with an enzyme detector, and calculate the hemolysis rate. The formula is as follows:

$$\text{Hemolysis}(\%) = \frac{\text{OD(sample)} - \text{OD(negative)}}{\text{OD(positive)}–\text{OD(negative)}} \times 100. \quad (3)$$

The *in vivo* metabolism and distribution of MPDA-HK@PDA-HA

Healthy 4–6-week-old SPF-grade female Balb/c mice were fasted for 12 h before the experiment and were kept with normal water supply. All mice were injected *via* tail vein with a dose of 20 mg/kg. Blood samples from each group of mice were collected from the carotid arteries at the following time points after administration: 1, 5, 15, and 60 min. Three mice were selected at each time point. The blood samples were collected in heparin sodium-treated centrifuge tubes, centrifuged at 4000 rpm/min for 10 min, and the upper plasma was aspirated and stored at −80 °C for later use. 100 μl of plasma was taken, and 300 μl of methanol protein precipitation was added. After

ultrasonication, the supernatant was collected and centrifuged at 12000 rpm/min, and the upper clear liquid was aspirated and stored for later HPLC analysis to determine the content of MPDA-HK@PDA-HA in the samples.

Antitumor effects of MPDA-HK@PDA-HA *in vivo*

All animal experiments have been approved by the Ethics Committee of the Chongqing Institute of Green and Intelligent Technology, Chinese Academy of Sciences (No. 2024.024). A Balb/c mouse (6–8 weeks old, female) breast cancer tumor model was established by subcutaneously injecting 100 μl 1×10^6 4T1 cells into the proper posterior back of Balb/c mice. When the tumor size was about 100 mm^3, the mice were randomly divided into five groups (n = 5): PBS, HK, MPDA+NIR, MPDA-HK@PDA-HA, and MPDA-HK@PDA-HA+NIR. The mice were intravenously injected *via* the tail vein with 100 μl (1 mg/ml) of the corresponding drug on day 1, followed by irradiation with an 808 nm near-infrared laser at a power density of 1 W/cm^2 for 5 min on day 2. This treatment regimen was repeated over a total period of 8 days. Tumor volume was monitored and recorded during treatment. The tumor volume is calculated as follows: $V = (a \times b^2)/2$, where "a" is the tumor length and "b" is the tumor width. To evaluate toxicity, the weight of the mice was measured and recorded every other day. After 8 days of treatment, the mice were killed, and tumor tissue was collected.

Antitumor effect of MPDA-HK@PDA-HA combined with Met *in vivo*

The modeling method for breast cancer mice is the same as before. The mice were randomly divided into five groups (n = 5), namely, PBS, MPDA-HK@PDA-HA, MPDA-HK@PDA-HA+NIR, MPDA-HK@PDA-HA+Met(20 mg/kg), and MPDA-HK@PDA-HA+Met (20 mg/kg)+NIR. The tail vein of 4T1 tumor-bearing mice was injected with 100 μl of different drug solutions (1 mg/ml), and the NIR group was irradiated with a laser for 5 min. The tumor volume was monitored and recorded during treatment, and the weight of the mice was measured and recorded every other day. After 8 days of treatment, the mice were killed, tumor tissues were collected, and the tumors were fixed with 4% paraformaldehyde and then sliced and embedded after dehydration. Tumor sections were stained by H&E, TUNEL, and Ki67 and then scanned.

Western blot analysis

Western blot was used to detect the presence of specific protein markers and autophagy/apoptosis-related proteins. After the protein glue was transferred to the PVDF membrane and closed with 5% BSA, the PVDF membrane was incubated at 4 °C overnight with the following primary antibodies (1:1000): caspase 3, PARP, cleaved caspase 3, cleaved PARP, and β-actin. After being completely washed, the membrane was incubated with a secondary antibody (1:2500) for 1 h. After being fully cleaned, the membrane was contacted with the ECL developer evenly and observed with a chemiluminescence imager.

MPDA-HK@PDA-HA+Met toxicity *in vivo*

The mice killed after treatment were dissected, the heart, liver, spleen, lung, and kidney were collected, and the toxicity of nanomaterials to major organs was observed by HE staining.

Statistical analysis

All experiments were replicated at least three times, all data were expressed as mean, and ANOVA and pair comparison by independent t-test determined standard deviation (SD) and statistical significance. $p < 0.05$ was considered statistically significant.

SUPPLEMENTARY MATERIAL

See the supplementary material for additional information on blood compatibility of MPDA-HK@PDA-HA (Fig. S1), the metabolism and distribution of MPDA-HK@PDA-HA in plasma, heart, liver, spleen, lung, and kidney were detected by HPLC (Fig. S2), antitumor activity of MPDA-HK@PDA-HA *in vivo* (Fig. S3), and HE staining images of major organs of mice were obtained after treatment (Fig. S4).

ACKNOWLEDGMENTS

This work was supported by the National Natural Science Foundation of China (No. 82472162), the Chongqing Natural Science Foundation General Project (No. CSTB2024NSCQ-MSX1294), the Fundamental Research Funds for the Central Universities (No. 2024CDJXY017), the National Health Commission's Medical Science and Technology Development and Research Center (Research Special Project on Post-marketing Clinical Studies of Innovative Drugs: No. WKZX2024CX103105), and the Shanghai Municipal Key Laboratory of Maternal and Fetal Medicine Open Research Fund (No. mfmkf202302).

AUTHOR DECLARATIONS

Conflict of Interest

The authors have no conflicts to disclose.

Ethics Approval

Ethics approval for experiments reported in the submitted manuscript on animal or human subjects was granted. All animal experiments have been approved by the Ethics Committee of the Chongqing Institute of Green and Intelligent Technology, Chinese Academy of Sciences (No. 2024.024).

Author Contributions

Qianqian Du, Qianfan Zhang, and Jialing Li contributed equally to this work.

Qianqian Du: Visualization (equal); Writing – original draft (equal); Writing – review & editing (equal). **Qianfan Zhang:** Visualization (equal); Writing – original draft (equal); Writing – review & editing (equal). **Jialing Li:** Visualization (equal); Writing – original draft (equal); Writing – review & editing (equal). **Xiaofei Wang:** Methodology (equal). **Xiangyu Gao:** Methodology (equal). **Guangyuan Tan:** Methodology (equal). **Qian Feng:** Methodology (equal). **Jigang Li:** Methodology (equal); Validation (equal); Writing – review & editing

(equal). **Yanchun Meng:** Funding acquisition (equal); Validation (equal); Writing – review & editing (equal). **Yongsheng Yu:** Conceptualization (equal); Funding acquisition (equal); Supervision (equal); Writing – review & editing (equal).

DATA AVAILABILITY

The data that support the findings of this study are available from the corresponding authors upon reasonable request.

REFERENCES

[1]B. Han, R. Zheng, H. Zeng, S. Wang, K. Sun, R. Chen, L. Li, W. Wei, and J. He, "Cancer incidence and mortality in China, 2022," J. Nat. Cancer Cent. **4**(1), 47–53 (2024).

[2]H. Sung, J. Ferlay, R. L. Siegel, M. Laversanne, I. Soerjomataram, A. Jemal, and F. Bray, "Global Cancer Statistics 2020: GLOBOCAN estimates of incidence and mortality worldwide for 36 cancers in 185 countries," CA-Cancer J. Clin. **71**, 209–249 (2021).

[3]R. Tang, J. Xu, W. Wang, Q. Meng, C. Shao, Y. Zhang, Y. Lei, Z. Zhang, Y. Liu, Q. Du, X. Sun, D. Wu, C. Liang, J. Hua, B. Zhang, X. Yu, and S. Shi, "Targeting neoadjuvant chemotherapy-induced metabolic reprogramming in pancreatic cancer promotes anti-tumor immunity and chemo-response," Cell Rep. Med. **4**(10), 101234 (2023).

[4]H. Petrowsky, R. Fritsch, M. Guckenberger, M. L. De Oliveira, P. Dutkowski, and P.-A. Clavien, "Modern therapeutic approaches for the treatment of malignant liver tumors," Nat. Rev. Gastroenterol. Hepatol. **17**(12), 755–772 (2020).

[5]G. Song, L. Cheng, Y. Chao, K. Yang, and Z. Liu, "Emerging nanotechnology and advanced materials for cancer radiation therapy," Adv. Mater. **29**(32), 1700996 (2017).

[6]D. Wang, Z. Zhang, L. Lin, F. Liu, Y. Wang, Z. Guo, Y. Li, H. Tian, and X. Chen, "Porphyrin-based covalent organic framework nanoparticles for photoacoustic imaging-guided photodynamic and photothermal combination cancer therapy," Biomaterials **223**, 119459 (2019).

[7]Q. Sun, F. He, H. Bi, Z. Wang, C. Sun, C. Li, J. Xu, D. Yang, X. Wang, S. Gai, and P. Yang, "An intelligent nanoplatform for simultaneously controlled chemo-, photothermal, and photodynamic therapies mediated by a single NIR light," Chem. Eng. J. **362**, 679–691 (2019).

[8]B. Xia, B. Wang, J. Shi, Y. Zhang, Q. Zhang, Z. Chen, and J. Li, "Photothermal and biodegradable polyaniline/porous silicon hybrid nanocomposites as drug carriers for combined chemo-photothermal therapy of cancer," Acta Biomater. **51**, 197–208 (2017).

[9]B. Nasseri, M. Turk, K. Kosemehmetoglu, M. Kaya, E. Pişkin, N. Rabiee, and T. J. Webster, "The pimpled gold nanosphere: A superior candidate for plasmonic photothermal therapy," Int. J. Nanomed. **15**, 2903–2920 (2020).

[10]H. Xu, Y. Zhang, H. Zhang, Y. Zhang, Q. Xu, J. Lu, S. Feng, X. Luo, S. Wang, and Q. Zhao, "Smart polydopamine-based nanoplatforms for biomedical applications: State-of-art and further perspectives," Coord. Chem. Rev. **488**, 215153 (2023).

[11]W. Wei, X. Zhang, S. Zhang, G. Wei, and Z. Su, "Biomedical and bioactive engineered nanomaterials for targeted tumor photothermal therapy: A review," Mater. Sci. Eng., C **104**, 109891 (2019).

[12]S. Batool, S. Sohail, F. Ud Din, A. H. Alamri, A. S. Alqahtani, M. A. Alshahrani, M. A. Alshehri, and H. G. Choi, "A detailed insight of the tumor targeting using nanocarrier drug delivery system," Drug Delivery **30**(1), 2183815 (2023).

[13]K. Yang, L. Feng, X. Shi, and Z. Liu, "Nano-graphene in biomedicine: Theranostic applications," Chem. Soc. Rev. **42**(2), 530–547 (2013).

[14]J. C. Wanstall and S. R. O'Donnell, "Vasodilator responses to dopamine in rat perfused mesentery are age-dependent," Br. J. Pharmacol. **98**(1), 302–308 (1989).

[15]R. Katai, I. Tsuneyoshi, J. Hamasaki, M. Onomoto, S. Suehiro, R. Sakata, and Y. Kanmura, "The variable effects of dopamine among human isolated arteries commonly used for coronary bypass grafts," Anesthesia Analgesia **98**, 915–920 (2004).

[16]Y. Yang, T. Zhang, and D. Xing, "Single 808 nm near-infrared-TRIGGERED multifunctional upconverting phototheranostic nanocomposite for IMAGING-GUIDED HIGH-EFFICIENCY treatment of tumors," J. Biophotonics **14**(9), e202100134 (2021).

[17]G. Yang, R. Lv, F. He, F. Qu, S. Gai, S. Du, Z. Wei, and P. Yang, "A core/shell/satellite anticancer platform for 808 NIR light-driven multimodal imaging and combined chemo-/photothermal therapy," Nanoscale **7**(32), 13747–13758 (2015).

[18]Z. Hou, M. Yang, L. Huang, S. Xin, H. Yang, and J. Hou, "Polydopamine-based nanospheres as nanoplatforms to kill Staphylococcus aureus and to promote wound healing by photothermal therapy," Front. Chem. **10**, 1111701 (2022).

[19]N. Chen, S. Yao, M. Li, Q. Wang, X. Sun, X. Feng, and Y. Chen, "Nonporous versus mesoporous bioinspired polydopamine nanoparticles for skin drug delivery," Biomacromolecules **24**(4), 1648–1661 (2023).

[20]M. Zhu, Y. Shi, Y. Shan, J. Guo, X. Song, Y. Wu, M. Wu, Y. Lu, W. Chen, X. Xu, and L. Tang, "Recent developments in mesoporous polydopamine-derived nanoplatforms for cancer theranostics," J. Nanobiotechnol. **19**(1), 387 (2021).

[21]Q. Guan, R. Guo, S. Huang, F. Zhang, J. Liu, Z. Wang, X. Yang, X. Shuai, and Z. Cao, "Mesoporous polydopamine carrying sorafenib and SPIO nanoparticles for MRI-guided ferroptosis cancer therapy," J. Controlled Release **320**, 392–403 (2020).

[22]Y. Xing, J. Zhang, F. Chen, J. Liu, and K. Cai, "Mesoporous polydopamine nanoparticles with co-delivery function for overcoming multidrug resistance via synergistic chemo-photothermal therapy," Nanoscale **9**(25), 8781–8790 (2017).

[23]C.-P. Yu, P.-Y. Li, S.-Y. Chen, S.-P. Lin, and Y.-C. Hou, "Magnolol and honokiol inhibited the function and expression of BCRP with mechanism exploration," Molecules **26**(23), 7390 (2021).

[24]J. Sharanya, A. Purushothaman, D. Janardanan, and K. Koley, "Theoretical exploration of the antioxidant activity of honokiol and magnolol," Comput. Theor. Chem. **1232**, 114460 (2024).

[25]H.-H. Wang, Y. Chen, C.-Y. Changchien, H.-H. Chang, P.-J. Lu, H. Mariadas, Y.-C. Cheng, and S.-T. Wu, "Pharmaceutical evaluation of honokiol and magnolol on apoptosis and migration inhibition in human bladder cancer cells," Front. Pharmacol. **11**, 549338 (2020).

[26]C. Chen, Q.-W. Zhang, Y. Ye, and L.-G. Lin, "Honokiol: A naturally occurring lignan with pleiotropic bioactivities," Chin. J. Nat. Med. **19**(7), 481–490 (2021).

[27]J. Xu and H. Xu, "Magnolol: Chemistry and biology," Ind. Crops Prod. **205**, 117493 (2023).

[28]Q. Zhang, J. Wang, D. Liu, W. Zhu, S. Guan, L. Fan, and D. Cai, "Targeted delivery of honokiol by zein/hyaluronic acid core-shell nanoparticles to suppress breast cancer growth and metastasis," Carbohydr. Polym. **240**, 116325 (2020).

[29]P. Aiello, S. Consalvi, G. Poce, A. Raguzzini, E. Toti, M. Palmery, M. Biava, M. Bernardi, M. A. Kamal, G. Perry, and I. Peluso, "Dietary flavonoids: Nano delivery and nanoparticles for cancer therapy," Semin. Cancer Biol. **69**, 150–165 (2021).

[30]Y. Lei, Y. Yi, Y. Liu, X. Liu, E. T. Keller, C.-N. Qian, J. Zhang, and Y. Lu, "Metformin targets multiple signaling pathways in cancer," Chin. J. Cancer **36**(1), 17 (2017).

[31]Y. Han and C.-W. Li, "Effect of metformin on PARP inhibitors-induced epithelial-mesenchymal transition and PD-L1 expression in triple-negative breast cancer," J. Clin. Oncol. **37**(15), 1063–1063 (2019).

[32]S. Wang, Y. Lin, X. Xiong, L. Wang, Y. Guo, Y. Chen, S. Chen, G. Wang, P. Lin, H. Chen, S.-C. J. Yeung, E. Bremer, and H. Zhang, "Low-dose metformin reprograms the tumor immune microenvironment in human esophageal cancer: Results of a phase II clinical trial," Clinical Cancer Res. **26**(18), 4921–4932 (2020).

[33]J. Hu, Y. Ding, B. Tao, Z. Yuan, Y. Yang, K. Xu, X. Li, P. Liu, and K. Cai, "Surface modification of titanium substrate via combining photothermal therapy and quorum-sensing-inhibition strategy for improving osseointegration and treating biofilm-associated bacterial infection," Bioactive Mater. **18**, 228–241 (2022).

[34]L. Yang, W. Peng, T. Du, M. Li, T. Gao, Z. Yang, W. Wang, X. Zhou, R. Li, Q. Yan, and R. Qi, "Hierarchical self-recognition and response in CSC and non-CSC micro-niches for cancer therapy," Biomaterials **308**, 122581 (2024).

[35]J. Shi, Y. Ren, J. Ma, X. Luo, J. Li, Y. Wu, H. Gu, C. Fu, Z. Cao, and J. Zhang, "Novel CD44-targeting and pH/redox-dual-stimuli-responsive core–shell

nanoparticles loading triptolide combats breast cancer growth and lung metastasis," J. Nanobiotechnology **19**(1), 188 (2021).
[36]X. Zhang, J. Zhou, T. Chen, Q. Li, L. Gu, Y. Pan, L. Zheng, F. Zhang, J. Chen, H. Zhang, Q. Gong, and W. Gu, "Modulating tumor-stromal crosstalk via a redox-responsive nanomedicine for combination tumor therapy," J. Controlled Release **356**, 525–541 (2023).
[37]T. Ma, X. Tian, B. Zhang, M. Li, Y. Wang, C. Yang, J. Wu, X. Wei, Q. Qu, Y. Yu, S. Long, J.-W. Feng, C. Li, C. Zhang, C. Xie, Y. Wu, Z. Xu, J. Chen, Y. Yu, X. Huang, Y. He, L. Yao, L. Zhang, M. Zhu, W. Wang, Z.-C. Wang, M. Zhang, Y. Bao, W. Jia, S.-Y. Lin, Z. Ye, H.-L. Piao, X. Deng, C.-S. Zhang, and S.-C. Lin, "Low-dose metformin targets the lysosomal AMPK pathway through PEN2," Nature **603**(7899), 159–165 (2022).